AIAA JOURNAL
Vol. 31, No. 1, January 1993

Measurements of Circulation and Vorticity in the Leading-Edge Vortex of a Delta Wing

K. D. Visser* and R. C. Nelson†
University of Notre Dame, Notre Dame, Indiana 46556

Cross-wire measurements of the flowfield above a 75-deg flat plate delta wing were performed at a centerline chord Reynolds number of 2.5×10^5. Surveys normal to the planform yielded velocity field data at incidence angles of 20 and 30 deg for a series of chordwise locations. The distribution of the velocity, axial vorticity, and circulation showed a strong conical behavior upstream of the breakdown region and away from the apex and trailing edge regions. Spanwise velocity and vorticity profiles through the core of the vortex upstream of breakdown were scaled with the local geometry. Prior to breakdown, the majority of the axial vorticity in the primary vortex was observed to be concentrated at the center of the vortex, in a region of about twice that of the subcore diameter. The influence of changes in the angle of attack on axial vorticity with the opposite sense, such as that found in the secondary vortex, was much less than the vorticity in the primary vortex. The growth of the vortex circulation with distance from the apex was approximately linear over the forward end of the planform. The rate of growth was observed to decrease, however, aft of the midchord location. Radial circulation distributions scaled with the local semispan and exhibited a logarithmic behavior with increasing distance from the subcore, implying the possibility of a strong dependence on the local Reynolds stresses. Finally, parameters derived from slender body theory are shown to correlate the circulation for wings of different sweep.

Nomenclature

A	= area element normal to chordwise vorticity
a	= vortex core radius of maximum tangential velocity
c	= chord
k_1	= Sychev parameter = $\delta \cot \alpha$
P	= pressure
Re	= Reynolds number
r	= radial direction
r_c	= vortex core radius
s	= semispan
s^*	= local semispan, $s(x/c)$
U_∞	= freestream velocity
U_{eff}	= effective velocity sensed by hot wire
V_i	= velocity in the ith direction
u, v, w	= velocity in the x, y, z directions, respectively
x	= chordwise direction
y	= spanwise direction
z	= direction normal to wing surface
α	= angle of attack
Γ	= circulation
δ	= ratio of semispan to chord, s/c
ε	= apex half angle
κ_1,κ_2	= hot-wire cooling rate coefficients
Λ	= sweep angle
ϕ	= angular direction
Ω_i	= vorticity in the i direction

Introduction

THE vortex structure above a delta wing, and more particularly the physical process by which the flowfield undergoes the rapid transition referred to as vortex breakdown, has been a topic of concern for many years. As fluid moves over the planform, it separates at the sharp leading edges forming free shear layers that curve upward and form counter-rotating vortices on the leeward side of the wing. Axial flow in the central core regions can attain velocities over three times the freestream value. Additional spanwise outflow is induced on the upper surface beneath the coiled vortex sheet and separates from the surface as it approaches the leading edge to form "secondary vortices."

The size and strength of the primary vortices increase with angle of incidence, resulting in a substantial nonlinear lift increment. The maximum lift of a delta wing is limited by a phenomenon known as vortex breakdown. This is typically characterized by an increase in vortex diameter and a decrease in the core's axial and circumferential velocity followed by large scale turbulent dissipation. The consequences of breakdown include loss of lift and a reduction in the magnitude of the nose down pitching moment.

Theoretical arguments to explain the occurrence of breakdown have been classified by Hall[1] into three categories: 1) Vortex breakdown is similar to the separation of a two-dimensional boundary layer[2–5]; 2) hydrodynamic instability results in the transition to postbreakdown flow[6]; and 3) an existence of a critical state occurs which causes breakdown to occur.[5,7–11]

The complexities of these vortical flows are such that a complete analytical solution is difficult to obtain. Presently, none of these concepts are sufficient to accurately predict vortex breakdown on a delta wing over a wide range of conditions. Computational results have been seen to correspond to experimental data; however, no theory exists which can yield the flow detail in the breakdown zone or universally predict breakdown locations which consistently compare with experimental results. Acquisition of empirical information is also subject to complications, such as resolving flow details in regions of high gradients.

The values of vorticity reported by several different investigators[12–17] using similar sweep geometry and the angles of attack reveal a variety of magnitudes.[14] Conventionally, the model root chord c and the freestream velocity U_∞ are used as scaling quantities. Employing the local semispan would account for local geometric changes due to sweep angle and allow for comparison of data taken at different chord stations. Furthermore, the highest derived vorticity values were found to correspond to the finest grid resolution, as might be expected.[14] Thus, simply using the maximum vorticity values as a means of comparison between flow-

Received Oct. 15, 1991; revision received June 12, 1992; accepted for publication June 26, 1992.

*Graduate Research Student, presently holding a National Research Council Associateship at NASA Langley Research Center, MS 454, Hampton, VA 23665. Member AIAA.

†Professor, Hessert Center for Aerospace Research, Department of Aerospace and Mechanical Engineering.

fields, without accounting for the measuring resolution, can lead to erroneous conclusions.

An understanding of the vorticity field behavior is crucial to a better understanding of the overall vortex physics. Several investigators have put forth ideas specifically concerned with aspects of vorticity and circulation. Lee and Ho[18] state that "a stationary leading-edge vortex is achieved only when the convection of vorticity along the core axis balances the vorticity generation from the boundary layer of the leading edge" and the swirl angle is an indicator of this balance. A reduction in the axial convection, via the adverse pressure gradient at the trailing edge of the planform, is concluded to cause vortex breakdown.

This could be extended to say that the vortex may have a limit on the maximum amount of vorticity per unit area at a given station. Ng[19] postulated that a critical vorticity concentration occurs above which the aerodynamic forces cannot maintain a stable vortex over the airfoil. If this concentration is exceeded, the vortex transitions to another state, such as post breakdown, to redistribute the excess vorticity. An increase in the angle of attack leads to a higher rate of generation of the axial vorticity component without an accompanying increase in the axial velocity. The subsequent increase in the vortex strength, therefore, leads to vortex breakdown.

The argument of a critical vorticity distribution can be substantiated in light of the work by Delery et al.[20] They examined the effects of an adverse pressure gradient on a vortex generated by a 75-deg sweep delta wing at $\alpha = 27.5$ deg. The vortex was allowed to enter a two-dimensional duct with movable flaps at the aft end enabling various pressure distributions to be created in the duct. Their results indicate that a maximum vortex strength, as given by the maximum swirl velocity ratio, is strongly dependent on the local freestream pressure gradient. This can also be interpreted that the maximum amount of vorticity or circulation at a given station is limited by the ability of the flow to move downstream, which in turn is regulated by the pressure gradient. Thus, the state of the vortex, with regard to its breakdown potential, could be described by a ratio of vorticity generation conditions to flow transport conditions

A hypothesis by Brown and Lopez,[21] based on physics governing a stagnant recirculating flow region in confined cylindrical flows, argues that breakdown mechanisms rely on the production of negative azimuthal vorticity. This results from a tilting and stretching of the predominantly axial vorticity vector Ω_x, shown in Fig. 1. Vorticity diffusion leads to a radial redistribution of the circulation and a stretching and tilting of vortex lines due to a local increase of the tangential velocity V_ϕ. A reduction in the initially positive azimuthal component of vorticity occurs with axial distance and the subsequent "inviscid breakdown" process develops.

In light of the preceding discussion, a systematic investigation was undertaken to examine the behavior of certain delta wing flowfield quantities in a chordwise direction. The growth of the circulation and vorticity, over the planform from the apex to the trailing edge, were felt to be of most interest as it has been indicated that an increase in the circulation will initiate a flow transition to the postbreakdown state. Evaluation of the spatial dependence of these quantities might indicate changes in their distributions that would signify the onset of breakdown, such as an asymptotic approach to a common nondimensionalized value.

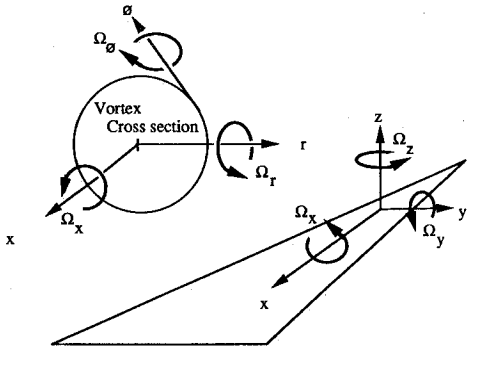

Fig. 1 Vortex geometry.

In the present investigation, velocity field data were acquired at a series of stations in the chordwise direction above a flat-plate delta wing, using a hot-wire technique described below. The spatial behavior of derived flowfield characteristics were then investigated. Specifically, vorticity and circulation distributions were derived and dimensional scaling was incorporated to examine the data for trends indicating breakdown was imminent. Additional data obtained using different measurement grid sizes, single wire core spectral data obtained upstream of breakdown, surface pressures, total pressures, and flow visualization were also acquired and details of these results are documented elsewhere.[22]

Experimental Procedures

All experiments were carried out in the University of Notre Dame subsonic wind-tunnel facilities. The tunnel is powered by an 18.6-kW ac induction motor which drives an eight-bladed 1.2 m (4 ft) fan located in the diffuser outlet. The four-degree-of-freedom, computer-controlled, probe-traversing test section is preceded by a 24:1 contraction inlet. Based on a single stepper motor pulse, the minimum step sizes possible in the streamwise, spanwise, and normal directions were 6.4, 25.4, and 20.8 μm, respectively. The positional accuracy of the system as a whole, however, was estimated at ± 1 mm.[12] The section dimensions were 610×610×1820 mm (24×24×76 in.).

The model used in this study, identical to that of Payne,[12] was a flat-plate delta wing having a windward 25-deg beveled edge, a root chord of 406.4 mm (16 in.), a thickness of 6.4 mm (0.25 in.), and a sweep angle of 75 deg. The maximum blockage at 30-deg angle of attack was under 6%. The minimum distance between the wing surface and the hot-wire probe was 3.0 mm due to probe geometry.

A TSI IFA 100 constant-temperature anemometer system was used to acquire the data in conjunction with a Macintosh II computer which in turn maneuvered the crosswire probe in the test section. The probes utilized 5-μm-diam tungsten wires giving a length/diameter ratio of 250. Overheat ratios were set to 1.8. The wires were calibrated during every test to reduce the possible errors associated with property changes of the wires. In addition, this procedure eliminated the need for temperature compensation as the ambient temperature did not vary by more than ± 1°C over the course of any individual test.

The use of a crosswire configuration generally assumes some knowledge of the flowfield, such as a known flow direction. The nature of the delta wing flow precludes any knowledge on the direction of the velocity vector everywhere in the field, save for the axial component upstream of the breakdown region. The technique of Sherif and Pletcher[23] was employed to derive the magnitudes of the velocity components, but their method does not give enough information to determine the direction. Use of their procedure requires two spatial measurements and is based on the effective velocity concept, that being that the wire senses a velocity composed of vectors normal and tangential to the wire which cool the wire at different rates κ_1 and κ_2. Jørgensen[24] has expressed the most general form of this equation as:

$$U_{\text{eff}}^2 = U_x^2 + \kappa_1^2 U_y^2 + \kappa_2^2 U_z^2 \tag{1}$$

for a crosswire lying in the xy plane. To fully determine the three velocity components and their associated directions in the present investigation, it was necessary to take four normal grid sweeps above the wing at each chordwise location, two for determining the magnitude, and two for direction. Since the direction of u could not be uniquely determined, the probe was kept in the flow forward of the breakdown region, and it was assumed that the direction of u was always in the positive x direction.

Two crosswire probe configurations were utilized and are shown in Fig. 2. The probes are similar geometrically, except for the sensing wire arrangements. Probe 1, a DISA 55P62, had wires lying in a plane perpendicular to the probe axis, whereas the wires of probe

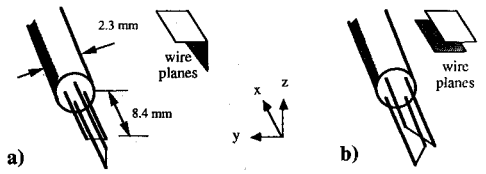

Fig. 2 Crosswire probe configurations: a) DISA 55P62 and b) DISA 55P6.

2, a DISA 55P61, were lying in a plane parallel to the probe axis, as shown by the accompanying schematic. The initial two grid sweeps used probe 1 with wire 1 at the reference of 0 deg and wire 2 at negative 90 deg. The probe was then rotated 45 deg about its axis and a second sweep initiated. This provided enough information for the velocity magnitudes to be determined.[23] The second probe was then required for two additional sweeps of the field, one with the plane of the wires parallel to the wing and one perpendicular to it. This second set of sweeps determined the direction of the transverse v and normal w velocity components.

Previous experiments have shown that the effect of introducing a probe into the flowfield does not greatly distort the flowfield provided the measurements are taken upstream of the breakdown zone. Payne et al.[25] examined the question of probe interference on the vortex velocity field measurements in a series of experiments using both an intrusive seven-hole pressure probe and nonintrusive laser Doppler anemometry (LDA). The influence of the probe on the vortex field was found to depend on the state of the vortex. If the wing angle of attack was below the angle where vortex breakdown would naturally occur over the wing, the intrusive probe was found to give accurate flowfield measurements when compared with the nonintrusive LDA measurements. On the other hand, if the breakdown was near the wing, then insertion of the seven-hole probe caused the breakdown to move upstream of the probe. When vortex breakdown occurred naturally between the wing midchord and apex, the intrusive probe was again found to provide accurate mean flow measurements of the postbreakdown flow.

In the present study, most of the detailed velocity measurements were made at an angle of attack of 20 deg, well below the onset angle of attack for vortex breakdown. In addition, flow-visualization studies were conducted to determine whether vortex breakdown occurred ahead of the hot-wire probe. The vortex core was marked with smoke and then the probe holder was moved through the vortex. At no time did the probe cause the flow to break down upstream of the probe. Furthermore, the probe was found to have little influence on the position of the vortex. That is, the vortex was found to be very stable and did not move away from the probe as the probe was traversed across the flowfield. In summary, the visualization studies conducted as part of this investigation and previous quantitative measurements[25] provided confidence that the present data accurately represented the flowfield characteristics.

Grid resolution was set to a y/s^* and z/s^* of 0.03 at each chord location. Since this represented 3.0% of the local semispan, the actual physical distance varied in each plane of data. At a station of $x/c = 0.5$ for example, $s^* = 54.4$ mm, and thus the grid resolution was 1.63 mm. At this station, the probe diameter of 2.3 mm translates to 4.2% of s^*. The probe holder, located 28 mm aft of the sensing wires, was 6 mm in diameter.

The performance of this cross-wire technique was evaluated by comparison with previous data obtained above the planform using a seven-hole probe (SHP)[12] as the inherent complexity of the equations[23] made an assessment of the error for each component difficult to isolate. Further comparisons of this measurement procedure, for configurations other than detailed below, can be found in Visser.[22]

Results and Discussion

The majority of data were accumulated over a 75-deg sweep delta wing at 20-deg angle of attack. Measurements were made at various chordwise stations in grid planes normal to the upper surface. Surveys were taken through the starboard vortex only, encompassing a z/s^* of 0.06 to approximately 1.0 and y/s^* from the chord centerline out to a spanwise location beyond the right edge of the wing. Data were also acquired at $\alpha = 30$ deg, however, aft of the $x/c = 0.5$ location the probe induced breakdown and thus only stations unaffected by the probe, upstream of this location, were measured. All tests were conducted at a centerline chord Reynolds number of 2.5×10^5.

The results of this study are divided into several sections. First, the velocities are discussed and compared with previously obtained data. The data are then analyzed in light of their vorticity characteristics. Dimensional scaling and various ways of interpreting the data are offered as a means for characterizing the behavior of the vortex. Circulation is then addressed and compared with the vorticity distributions. Finally, correlations of the data are presented.

Velocity

A typical axial velocity distribution measured by the present technique at an angle of attack of 20 deg and $x/c = 0.5$ is given in Fig. 3. Distances in the y and z directions are scaled by the local semispan and, hence, a $y/s^* = 1.0$ corresponds to the leading edge of the wing. The axial velocity u/U_∞ is the velocity normal to the measurement plane, which was perpendicular to the chord line, at the given chordwise station. The jetting core structure of the vortex is quite well defined, with the majority of the measured field maintaining a velocity above the freestream velocity.

The velocity data were compared to previous SHP data, for the same test conditions, obtained by Payne.[12] In general, it compared well; however, several differences are observed. The cross-wire data exhibited a peak axial velocity of $u/U_\infty = 2.33$, which is about 6% greater than that indicated in the SHP data. The core locations of $y/s^* = 0.69$ and $z/s^* = 0.40$, based on the position of maximum velocity for the cross-wire data, were further outboard and away from the wing than the SHP data of $y/s^* = 0.62$ and $z/s^* = 0.34$. This difference is believed to be probe induced, the cross-wire probe holder diameter, aft of the hot wire probe itself, being about twice as larger as the seven-hole probe. The core location for the seven-hole probe data, based on the position of the lowest value of the total pressure coefficient, was located at $y/s^* = 0.66$. The grid resolution of the SHP data was 4% of s^* in both directions, which, if applied to the core location at $y/s^* = 0.66$, would encompass both the $y/s^* = 0.62$ of the SHP velocity contour and $y/s^* = 0.69$ of the cross-wire data.

Core velocity profiles, those being the spanwise profiles of u/U_∞ and w/U_∞ at the z/s^* location corresponding to the maximum axial velocity, are presented in Fig. 4. The axial and tangential components obtained from the traverses are overlaid for chordwise stations of $x/c = 0.3$ to 0.8. Each profile is scaled by its local span s^*. Since the profiles exhibit similar characteristics, both in shape and magnitude, the flowfield in this region is seen to be scaling in a linear fashion, indicative of a conical behavior. The largest differences occur outboard of the core location. For consistency, every spanwise pass for each survey was made in the direction from the chord centerline to the leading edge. As stated earlier, the vortex did not move away from the probe; however, when the probe encounters the subcore region, there is a stronger tendency to "nudge" the solid-body-like subcore slightly before entering the region. This could result in a displacement of the core laterally, and

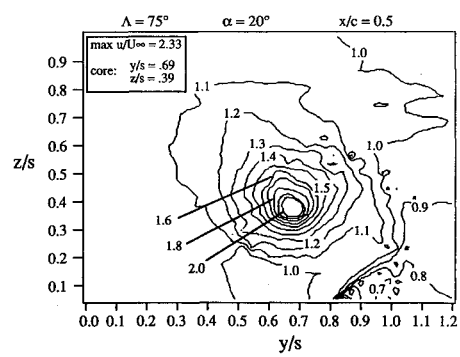

Fig. 3 Dimensionless axial velocity.

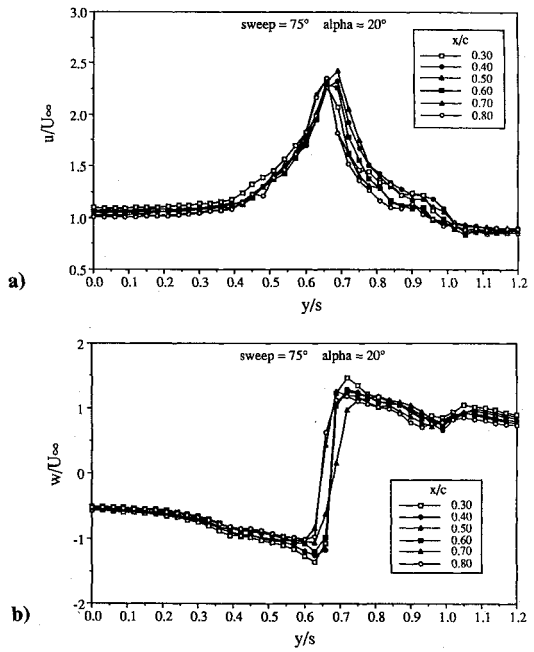

Fig. 4 Core velocity profiles: a) axial and b) tangential.

account for the variation in position of the peak velocity. Note also that each velocity profile in Fig. 4 represents the z/s^* location where the maximum u/U_∞ value was recorded. Because of the finite grid resolution, this may not be the actual maximum in that survey plane. The same implications apply for the tangential velocities in Fig. 4b.

Vorticity

The spatial progression of the vorticity was first examined in light of both its positive and negative components by central differencing the velocity field to obtain the axial vorticity component:

$$\Omega_x = \frac{\partial w}{\partial y} - \frac{\partial v}{\partial z} \tag{2}$$

The local spanwise distance was again used to scale the results, along with the freestream velocity, to examine the effect of the local geometry.

The resulting vorticity field for the $\alpha = 20$ deg data of Fig. 3 is presented as a contour plot in Fig. 5. The majority of the axial vorticity is concentrated in the region immediately around the core of the primary vortex. The extent of this region is approximately $y/s^* = 0.55$ to 0.75 and $z/s^* = 0.3$ to 0.5, or approximately 20% of the span. Note that this area is about twice the diameter of the subcore region in Fig. 4b, typically defined as the distance between the maximum tangential velocity components. Outside of this regime, the flow presents itself as essentially free of the positive axial vorticity component. A smaller region of flow with vorticity of the opposite sign and a much lower magnitude is located in the vicinity of the secondary vortex, marked by the dashed contours.

The vortex has been previously postulated to remain in the prebreakdown state if the amount of vorticity, or circulation, present is below a certain level. Since simply determining the maximum value of the vorticity does not make a definitive statement of the status of the vortex at that chord station, the axial vorticity distributions were integrated at each chordwise location to examine this hypothesis.

The behavior of the positive and negative values of the axial vorticity at each survey plane were examined by integrating the vorticity separately over their respective areas of influence. Both integrated components displayed an increase in magnitude with distance from the apex. In contrast to the positive component, the amount of negative vorticity present was observed to be similar for both angles of incidence. The data were scaled by s^* and the results are shown for each chord station in Fig. 6. The integrated vorticity components both show an almost linear growth with distance from the apex; however, the positive vorticity growth rate is decreasing slightly over the rearward part of the planform for the $\alpha = 20$ deg configuration. Note that the three planes of data taken in the prebreakdown flow at $\alpha = 30$ deg do not provide enough evidence to support the argument that breakdown occurs as a result of a total amount of vorticity being reached at a given station.

The chordwise behavior of the vorticity was further examined using the velocity profiles taken through the vortex core. Under the assumption that the radial velocity and its gradient were negligible compared to the other terms, the axial vorticity based on a single traverse through the core is defined as

$$\Omega_x = \frac{V_\phi}{r} + \frac{\partial V_\phi}{\partial r} = \frac{w}{r} + \frac{\partial w}{\partial r} \tag{3}$$

using polar coordinates. The axial core vorticity profiles for the $\alpha = 20$ deg configuration are overlaid for each of the measured x/c locations in Fig. 7a. Similar profiles are seen to exist at each station. As already mentioned, the majority of the axial vorticity component was contained within 20% of the semispan, dropping to less than 10% of the peak value for $r/s^* > \pm 0.10$ about the core center location. The vorticity data at the angle of attack of 20 deg scales in the same manner as the axial velocity profiles, that is, linearly with distance from the apex, which indicates a conical behavior of the flowfield. Similar distributions for $\alpha = 30$ deg gave no indication, such as a noticeably changing peak value or distribution, of the imminent breakdown present at $x/c > 0.5$.

The vorticity profiles in Fig. 7a were then nondimensionally integrated along each respective semispan to derive a set of values indicative of the local vorticity density distribution. These values are given in Fig. 7b. As might be expected from Fig. 7a, the $\alpha = 20$ deg no breakdown case revealed a relatively constant value for all of the integrated profiles in the chordwise direction. The single SHP point, derived from Payne (1987), for the $\Lambda = 75$ deg, $\alpha = 20$ deg configuration falls at the lower edge of the band of this data. Scatter in the data is attributed to the lack of resolution in obtaining the peak vorticity value along the vortex axis.

The observed behavior of the axial vorticity strongly supports the conical nature of the delta wing vortex in the region preceding

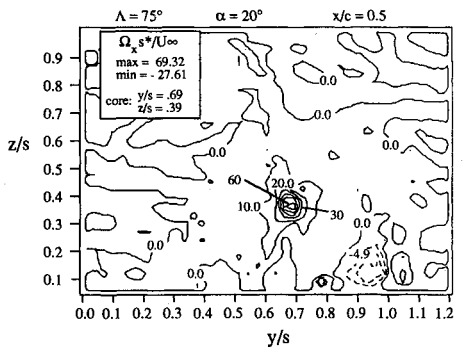

Fig. 5 Dimensionless axial vorticity.

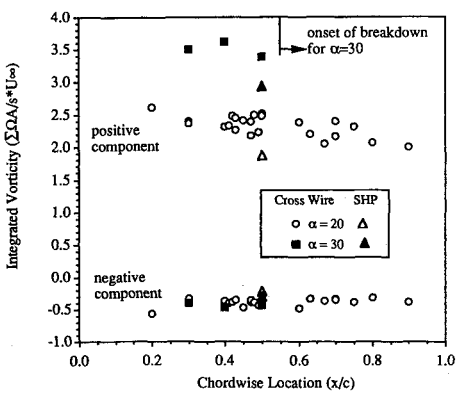

Fig. 6 Integrated vorticity.

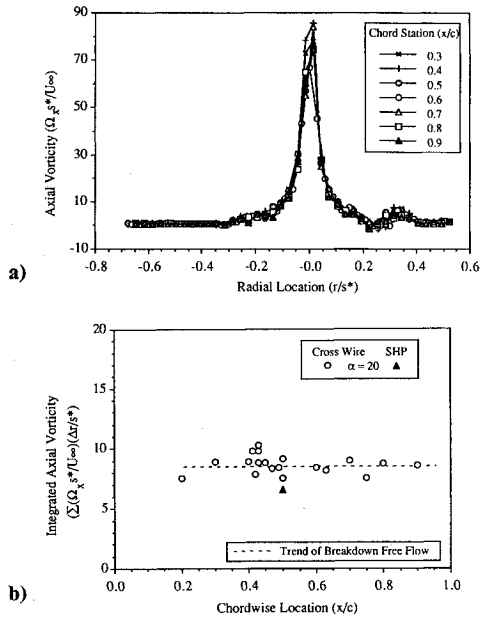

Fig. 7 Axial vorticity: a) core profiles and b) integrated values.

breakdown. Scaling both the maximum vorticity values and the profiles based on a traverse through the core by the local spanwise geometry indicates that the distribution of the axial vorticity through the core is similar at each chordwise station. The vorticity components were arrived at using calculations based on differentiating the experimental data. Circulation is derived from an integration process, resulting in a possible reduction of error, and thus the data were further analyzed in this manner.

Circulation

The circulation Γ was calculated from the crossflow velocity components, in the plane of the survey grids, and is compared with the spatially integrated vorticity field distribution for the 20-deg incidence case in Fig. 8. The values have been nondimensionalized by the freestream velocity and the root chord. They are plotted outward from the core center ($r = 0$), where the radial distance has been scaled by the local semispan. Each curve represents a chordwise location and the circulation is seen to grow in a chordwise manner. This is what one would expect, as more of the feeding sheet is being wrapped into the vortex with increasing distance from the apex. The circulation is seen to increase at a decreasing rate from the center of the vortex and reaches a maximum inside of the planform's leading edge. The profiles gain an additional rise in circulation as the integration path encloses the shear layer outboard of the leading edge.

The circulation and integrated vorticity profiles are seen to correspond quite well, indicating that errors associated with differentiating the discrete velocity field data were not substantial. It should be noted that the circulation was not calculated along paths corresponding to a constant radius from the core center. Instead, square integration paths were followed which enclosed a path of constant radius. For distances greater than the distance of the vortex axis to the planform, the lower integration path was bounded by the wing surface. The uncertainty in the calculated circulation values, based only on the error in spatial measurement, was estimated to be less than 0.25% at $x/c = 0.5$. The associated error in the corresponding vorticity calculations was approximately twice that amount. No account is made of the error associated with the calculated velocity in either case, due to the four sweep method.

To examine the dependence on distance from the apex, the circulation values were scaled by the local semispan s^*. This had the effect of bringing the curves for a given angle of attack close together. The agreement of the resulting scaled profiles implied that the circulation at a constant angle of attack is increasing in direct proportion to the local semispan. This linear increase of circulation in a chordwise direction at any particular radius supports the conical nature flowfield assumption. To account for the difference in attack angle, some function of α as a scaling parameter can be incorporated. As an example, the circulation values for three x/c locations are further scaled by $\sin(\alpha)$, which can also be interpreted as scaling by the component of the freestream velocity normal to the planform. The results, plotted in Fig. 9, do not collapse to a line, but rather a band. A universal curve of the form suggested in Fig. 9 would be very useful, however it is difficult to ascertain the error present in each profile without a more extensive database.

A closer look at Figs. 8 and 9 indicates the growth of the circulation with increasing distance from the vortex axis to be nonlinear at first, followed by a leveling off, and then the subsequent increase as the shear layer is encountered. Further insight on the nature of this rotational region can be gained from the work of Hoffmann and Joubert[26] on turbulent line vortices. Based on their analysis of the equations of motion, utilizing the assumption that the inertia terms are negligible compared to the Reynolds stress terms, a circulation distribution of the form below was derived:

$$\Gamma/\Gamma(a) = A\,[ln\,(r/a)\,] + 1 \qquad (4)$$

This equation applies in the vortex outside of the subcore region, where a represents the radius of maximum tangential velocity, A some constant, and $\Gamma(a)$ the circulation at the core radius a. They also obtained experimental data at a series of downstream stations for a vortex generated by a differential airfoil, suggesting a universal circulation distribution exists with $A = 0.93$.

The circulation distributions, scaled by the local semispan, are plotted in Fig. 10 using a logarithmic scale for the radius. Evidence of the behavior with radius for a turbulent vortex is indicated by the apparent logarithmic region before the shear-layer flow is encountered. The slopes of the profiles are different for each angle of attack, as might be expected from the different rates of circulation growth. Keeping in mind that the sensitivity of the indicated slope is large due to the logarithmic nature of the plot, $\Gamma(a)$ and the associated slope were estimated from the profiles in Fig. 10 to compare to Hoffmann and Joubert. Using $a = 0.05$ as an approxi-

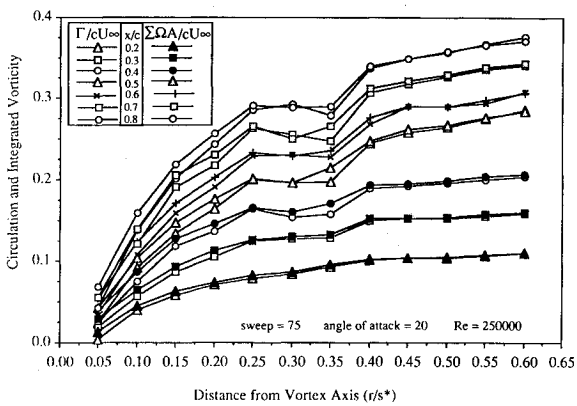

Fig. 8 Radial distribution of circulation and integrated vorticity.

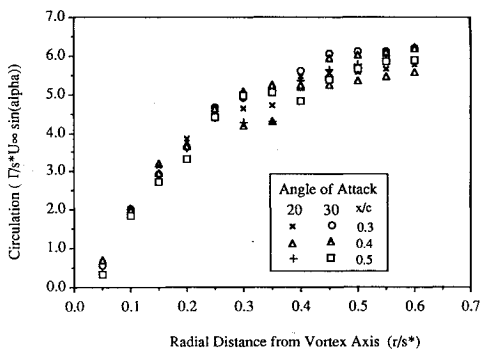

Fig. 9 Effect of scaling on the radial variation of circulation.

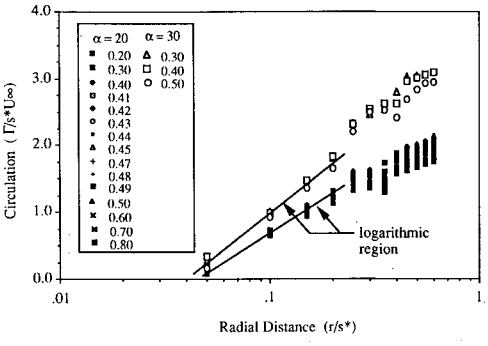

Fig. 10 Dependence of circulation on logarithmic radial position.

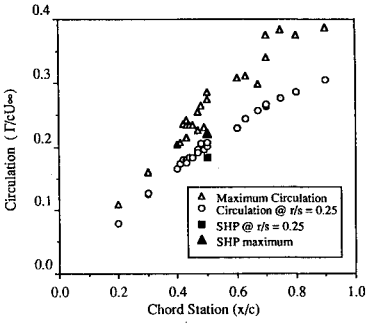

Fig. 11 Chordwise variation of circulation at α = 20 deg.

mate subcore radius, based on Fig. 4b, values of $\Gamma(a) = 0.08$ and 0.21 for α=20 and 30 deg, respectively, were estimated yielding associated values of A=10.8 and 5.2. Although no simple dependence on angle of incidence was found, such as sin(α), these values were seen to be represented approximately by $A=1.3/\sin^2(\alpha)$.

The profiles in Figs. 8–10 illustrate the radial dependence of the circulation. To assess the chordwise variation of the vortex strength, the maximum value of the circulation at each survey station, scaled by the chord, was plotted for the α = 20-deg case in Fig. 11. Despite the scatter, the data corresponding to the maximum radius of integration of $r/s^* = 0.6$, denoted by the Δ symbols, appear to indicate a linear behavior forward of the midchord. The scatter may be attributable to probe interference at the lower boundary of the integration path, since this corresponds to the upper surface of the wing for r/s^* distances greater than the z/s^* location of the vortex axis. The proximity of the probe to the wing surface could severely alter local measurements of the spanwise velocity components and thus the resulting magnitude of the circulation at each x/c station.

A better representation of the behavior of the vortex is obtained if the circulation values at the radial location where the profile of Fig. 8 initially levels off are plotted, that being approximately $r/s^* = 0.25$. The circulation values at this radial distance have also been plotted in Fig. 11. A much smaller scatter is present in the data. The values also appear to follow an approximately linear distribution over the middle-to-forward portion of the planform. As the aft end of the wing is approached, a decrease in the growth rate of the circulation is seen and a leveling off occurs. This further supports the arguments pertaining to the conical behavior of the delta flowfield, at least over the midportion of the wing, since a conical flowfield demonstrates the linear growth of circulation in a chordwise direction.[27] The SHP data falls below the cross-wire for both the $r/s^* = 0.6$ and the 0.25 radii. Again, this may be due to the increase in grid resolution of the cross-wire data.

The characteristics of the circulation through the breakdown region cannot be addressed with the present data, since no measurements were taken there. Seven-hole probe data have been obtained by Payne[12] above a Λ = 85 deg for α = 40 deg planform at several stations directly in the breakdown region. Derived circulation values from this data at $r/s^* = 0.25$ and 0.7 were scaled by the

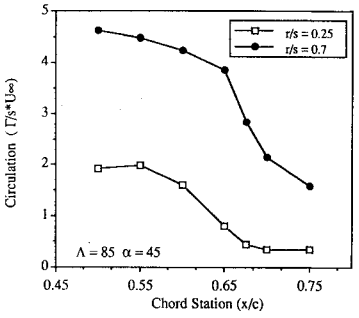

Fig. 12 Circulation distribution through breakdown.

s^* and are presented in Fig. 12. Although the circulation might be expected to remain constant when scaled by the local semispan, as implied by the growth trends in Fig. 11, they are seen to fall through the breakdown region. Since the measured circulation in this direction is directly related to the axial vorticity component, either the axial vorticity has been redistributed or it has become less. This is consistent with the theory of Brown and Lopez,[21] who postulated that the predominantly axial vorticity vector rotates away from the axial direction to a predominantly tangential direction at breakdown. A rotation of the vorticity vector to the radial or tangential direction would explain the drop in the values of calculated circulation.

The range of angles of incidence and sweep angles investigated by Payne[12] also allows the dependence of circulation on these variables to be examined. Circulation values at a chordwise location of $x/c = 0.5$ are presented in Fig. 13. Both the results for $r/s^* = 0.25$ and for the entire grid survey at each station are presented. The circulation is seen to grow in a near linear manner for each configuration with incidence, as indicated in Fig. 13a. The profiles also indicate an apparent linear dependence of the circulation on sweep angle for a given angle of attack. Eventually, the breakdown moves ahead of the $x/c = 0.5$ station and the circulation values drop in the same manner as was pointed out in Fig. 12. This again seems to support the argument[21] that the longitudinal or axial vorticity component loses some intensity to some other direction.

It could be alternatively surmised that the expansion of the core simply spreads out the vorticity and that maintaining the same integration path, of say $r/s^* = 0.25$ in Fig. 13a, would thereby result in the lower circulation values. Vorticity is still being added to the vortex structure, via the shear layer along the entire leading edge, and this would continue to increase the circulation in the chordwise direction. The maximum circulation is shown in Fig. 13b and was found to continue to increase as distance increased from the apex past the point of breakdown. The broken line in Fig. 13b is just a visual marker to connect the angles at which breakdown moved forward of the $x/c = 0.50$ location for that geometry. Thus, it could be concluded that it is not just the total amount of circulation present which determines whether the vortex breaks down or not, but it is the local concentration of that vorticity which gives rise to the breakdown.

The observed behavior of the circulation agrees with the axial vorticity and velocity distributions in indicating that a near conical flowfield exists for the majority of the prebreakdown leading-edge vortex. The flow scales with the local geometry, and to a lesser extent with the sine of the angle of incidence. The strength of the vortex, as defined by the circulation in the yz plane, increases in a near linear manner with angle of attack for a fixed chord location and with distance from the apex over the forward region of the planform. This increase in strength is inevitably followed by breakdown which reduces the concentration of axial vorticity about the vortex axis. The onset of breakdown cannot be solely attributable to the total vortex strength in absolute terms, for the total circulation of the vortex is still increasing with x/c, even after breakdown. Instead, it is believed that the local circulation taken about the core region plays a most significant role in the onset of breakdown. There is a sharp decrease in this value after breakdown, presumably in a nonreversible manner, for the flow never

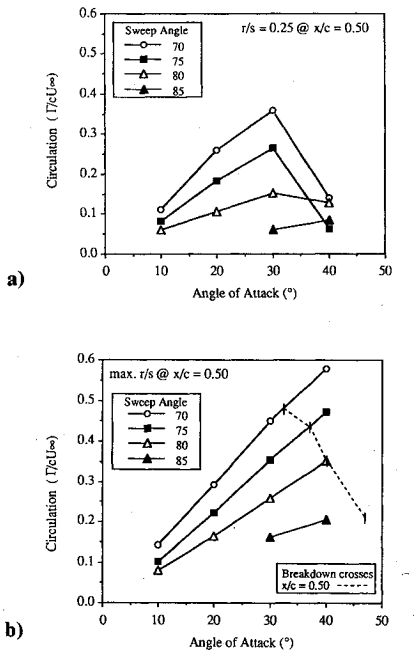

Fig. 13 Dependence of circulation on sweep and incidence: a) *r/s* = 0.25 and b) maximum.

transitions to the prebreakdown state. It should be emphasized that there are other flow parameters which have an influence on the breakdown and have not been accounted for here. The circulation was determined solely from the velocity flowfield without consideration of the influence of, say, the pressure gradient variations or the axial velocity component.

Vortex Strength Correlation

Parameters can be defined to incorporate external conditions, such the sweep angle and angle of attack, along with the measured flowfield properties in an effort to determine what if any interaction occurs as breakdown is approached spatially. This approach has already been utilized, to a certain extent, by scaling the field properties by the local semispan and even the sine of the angle of attack. A more direct line of reasoning was incorporated by Hemsch and Luckring[28] in a correlation for the measured vortex circulation. Their relation utilizes a parameter derived by Sychev[29] in his Euler analysis of flow about an arbitrary slender body. Sychev assumed

$$\delta = s/c << 1$$

and obtained an approximate set of equations for the inner region of the flow involving only the parameter $k_1 = \delta \cot \alpha$. Hemsch and Luckring[28] used this Sychev parameter to correlate the strength of a delta wing vortex at the trailing edge in the form of

$$g = \frac{\Gamma}{U_\infty c \tan^2 \varepsilon \cos \alpha} = AK^n \mu \qquad (5)$$

where

$$K = \tan \alpha / \tan \varepsilon = 1/k_1$$

for some constant values of n and A. By plotting g and K in a log-log format, they demonstrated that a fit of the form $g = AK^{1.2}$ was seen for data obtained from Wentz and MacMahon,[30] $\Lambda = 62$ deg, and that of Delery et al.[20] Values of g and K ranged from 0.5 to 10.0 and 0.2 to 2.0, respectively. A value of $n = 1.2$ was seen to accurately fit the numerical conical slender body theory of Smith.[31]

The data from this investigation were also plotted in this manner but the expected collapse of data was not immediately evident. Hemsch and Luckring[28] used data that were acquired in the wake of the models. Since the present tests were conducted at locations

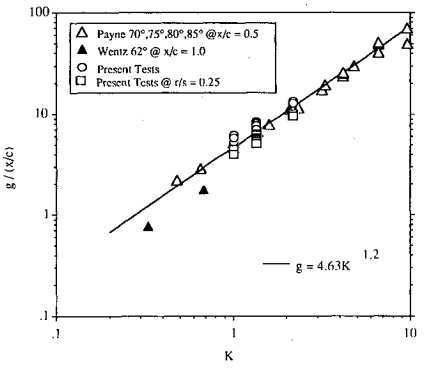

Fig. 14 Sychev parameter based correlation of Hemsch and Luckring.

above the wing surface, a further scaling of g by the local chord ratio x/c was found to bring the data into line with theory for $A = 4.63$ as shown in Fig. 14. The seven-hole probe data of Payne[12] were also scaled by x/c and are presented in Fig. 14 along with that of Wentz and MacMahon.[30] Payne's data represent sweep angles of 70, 75, 80, and 85 deg at various chord locations. It is seen to extend the theoretical line of Smith[31] to a g of 100 and a K of 10. Thus, it would appear that this relation strongly correlates the vortex strength with the angle of attack and the wing geometry.

If Eq. (5) is manipulated to include the ratio x/c and expressed in terms of s^*,

$$g = \Gamma / U_\infty s^* \tan \varepsilon \cos \alpha \qquad (6)$$

Further division of g by K yields the constant A expressed as

$$A = \frac{\Gamma (\tan \varepsilon \cos \alpha)^{n-1}}{U_\infty s^* (\sin \alpha)^n}$$

or

$$A = \frac{\Gamma (\tan \varepsilon \cos \alpha)^{0.2}}{U_\infty s^* (\sin \alpha)^{1.2}}$$

for $n = 1.2$, which would be a function of distance from the vortex axis or a constant at a given nondimensionalized radius for each chord station. Note that by setting n equal to 1 in the preceding expression, this function reduces to that used in Fig. 9b.

Conclusions

The preceding discussion strongly supports the argument that the flow over a delta wing, upstream of the breakdown regions and away from the apex and trailing-edge regions, behaves in a conical manner in that properties remain constant along rays emanating from the apex. Spanwise vorticity and velocity distributions based on a single traverse through the core of the vortex scale with the local geometry in the prebreakdown state. Dimensional scaling of the radial circulation distribution by the local semispan also indicates this flow property to be similar at each chordwise location upstream of breakdown. Thus the local semispan represents a viable length scale for flat-plate delta planforms.

The conical nature of the properties just noted occurs most strongly over the central portion of the planform, that is, away from the apex and trailing-edge regions. Near the apex, the geometry of the flat-plate delta wing is such that the span of the wing is on the order of the thickness and the fluid senses a blunt body rather than a slender, thin planform. In the same manner, the field is altered as it approaches the trailing edge by the pressure recovery of the flow.

Further evidence of the conical behavior of the flowfield is supplied by the approximately linear increase in strength of the vortex with distance from the apex over the forward area of the wing. The circulation was also found to increase linearly with angle of incidence for a fixed chordwise station. The parameter derived by

Hemsch and Luckring, based on Sychev slender-body assumptions, incorporates both the effects of sweep and angle of attack to provide a strong correlation of the vortex strength over a wide range of test conditions. Inclusion of the relative chord location x/c as shown in the present study accounts for regions where the vortex size and strength are increasing, such as over a delta wing.

Since this increase in vortex strength is inevitably followed by breakdown, and the circulation continues to grow aft of this region, it is surmised that it is not just the total amount of circulation present which determines whether the vortex breaks down or not, but it is the concentration of that circulation, associated with the axial vorticity direction, which gives rise to the breakdown.

Several other conclusions were reached and are summarized below:

1) The use of the present cross-wire technique, employing four spatial passes and two different probe configurations for a single survey, was satisfactory in measuring the flow velocities.

2) Employing the maximum value of axial vorticity in determining the local strength or state of the vortex structure is deceptive. Grid-resolution dependence and the locally steep gradients deter this type of quantification.

3) The majority of the prebreakdown positive axial vorticity is concentrated about the vortex axis in a region approximately twice the diameter of the subcore.

4) Adjustment of the flowfield to changing test conditions occurred for the most part in the positive axial vorticity regions. The negative axial vorticity distributions, concentrated in the secondary vortex region, did not change significantly with distance from the apex for both angles of attack investigated.

5) The circulation profiles exhibited a logarithmic dependence over a given radial distance from the vortex axis pointing to a possibly substantial influence of Reynolds stress terms in the flowfield.

It is hoped that these results, such as the suggested implications of the Reynolds stresses, will provide useful information and insight in modeling delta wing flows, examining experimental and numerical data, and offering direction for further measurements.

Acknowledgments

The authors gratefully acknowledge the support of the NASA Langley Research Center, Grant NAG-1-1156, and the University of Notre Dame for this research effort.

References

[1]Hall, M. G., "Vortex Breakdown," *Annual Review of Fluid Mechanics,* Vol. 4, 1972, pp. 195–217.

[2]Gartshore, I. S., "Recent Work In Swirling Incompressible Flow," NAE Aeronautical Rept. LR-343, National Research Council, Canada, June 1962.

[3]Stewartson, K., and Hall, M.G., "The Inner Viscous Solution for the Core of a Leading-Edge Vortex," *Journal of Fluid Mechanics,* Vol. 15, Feb. 1963, pp. 306–318.

[4]Hall, M. G., " The Structure of Concentrated Vortex Cores," *Progress in Aeronautical Sciences,* Vol. 7, edited by D. Kuchemann et al., Pergamon Press, 1966, pp. 53–110.

[5]Grabowski, W. J., and Berger, S. A., "Solutions of the Navier Stokes Equations for Vortex Breakdown." *Journal of Fluid Mechanics,* Vol. 75, June 1976, pp. 525–544.

[6]Ludweig, H., "Contribution to the Explanation of the Instability of Vortex Cores Above Lifting Delta Wings," Aero. Versuchsanstalt, Gottingen, Rept. AVA/61 A01, 1961.

[7]Squire, H. B., "Analysis of the 'Vortex Breakdown' Phenomenon," Aero. Dept., Imperial College, Rept. 102, London, 1960.

[8]Benjamin, T. B., "Theory of Vortex Breakdown Phenomena," *Journal of Fluid Mechanics,* Vol. 14, Dec. 1962, pp. 593–629.

[9]Bossel, H. H., "Vortex Breakdown Flowfield," *Physics of Fluids,* Vol. 12, No. 3, 1969, pp. 498–508.

[10]Randall, J. D., and Leibovich, S., "The Critical State: A Trapped Wave Model of Vortex Breakdown," *Journal of Fluid Mechanics,* Vol. 58, May 1973, pp. 495–515.

[11]Escudier, M. P., and Keller J. J., "Vortex Breakdown: A Two Stage Transition," Paper 25, AGARD-CP-342, April 1983.

[12]Payne, F. M., "The Structure of Leading Edge Vortex Flows Including Vortex Breakdown," Ph.D. Dissertation, Univ. of Notre Dame, Notre Dame, IN, May 1987.

[13]Kjelgaard, S. O., and Sellers, W. L. III, "Detailed Flowfield Measurements over a 75° Swept Delta Wing for Code Validation," Paper 10, AGARD Symposium on Validation of Computational Fluid Dynamics, CP-437, Vol. 2, May 1988.

[14]Nelson, R. C., and Visser, K. D., "Breaking Down the Delta Wing Vortex—The Role of Vorticity in the Breakdown Process," Paper 21, AGARD Symposium on Vortex Flow Aerodynamics, CP-494, Oct. 1990.

[15]Verhaagen, N., and van Ransbeeck, P., "Experimental and Numerical Investigation of the Flow in the Core of the Leading Edge Vortex," AIAA Paper 90-0384, Reno, NV, Jan. 1990.

[16]Carcaillet, R., Manie, F., Pagan, D., and Solignac, J. L., "Leading Edge Vortex Flow Over a 75 Degree-Sweep Delta Wing—Experimental and Computational Results," Proceedings of the 15th Congress of the International Council of the Aeronautical Sciences, London, Sept. 1986, pp. 1–15.

[17]Pagan, D., and Solignac, J. L., "Experimental Study of the Breakdown of a Vortex Generated By a Delta Wing," *La Recherche Aérospatiale,* No. 3, May–June 1986, pp. 29–51.

[18]Lee, M., and Ho, C. M., "Vortex Dynamics of Delta Wings," *Frontiers in Experimental Fluid Mechanics, Lecture Notes in Engineering,* Vol. 46 Springer-Verlag, Berlin, 1989, pp. 365–427.

[19]Ng, T. T., "On Leading Edge Vortex and Its Control," AIAA Paper 89-3346, Boston, MA, Aug. 1989.

[20]Delery, J., Pagan, D., and Solignac, J. L., "On the Breakdown of the Vortex Induced by a Delta Wing," *Colloquium on Vortex Control and Breakdown Behavior,* Baden, Switzerland, ONERA TP 1987-105, April 1987, pp. 1–25.

[21]Brown, G. L., and Lopez, J. M., "Axisymmetric Vortex Breakdown Part II: Physical Mechanisms," *Journal of Fluid Mechanics,* Vol. 221, Dec. 1990, pp. 553–576.

[22]Visser, K. D., "An Experimental Analysis of the Critical Factors Involved in the Breakdown Process of Leading Edge Vortex Flows," Ph.D. Thesis, University of Notre Dame, Notre Dame, IN, April 1991.

[23]Sherif, S. A., and Pletcher, R. H., "A Normal-Sensor Hot Wire/Film Probe Method for the Analysis of Highly Three-Dimensional Flows," *ASME Applied Mechanics Biomechanical and Fluid Engineering,* FED Vol. 49, June 1987, pp. 19–22.

[24]Jørgensen, F. E., "Directional Sensitivity of Wire and Fiber-film Probes—An Experimental Study," DISA Information, No. 11, May 1971.

[25]Payne, F. M., Ng, T. T., and Nelson, R. C., "Probe Interference on Measurement of Leading Edge Vortex Flows," *Experiments in Fluids,* Vol. 7, No. 1, 1989, pp. 1–8.

[26]Hoffmann, E. R., and Joubert, P. N., "Turbulent Line Vortices," *Journal of Fluid Mechanics,* Vol. 16, July 1963, pp. 395–411.

[27]McCune, J. E., and Tavares, T. S., "Unsteady 3-D Aerodynamics of Slender Wings in Severe Maneuver," *Proceedings of the 1st National Fluid Dynamics Congress,* (Cincinnati, OH), 88-3543-CP, Pt. 2, July 1988, pp. 815–824.

[28]Hemsch, M. J., and Luckring, J. M., "Connection between Leading Edge Sweep, Vortex Lift and Vortex Strength for Delta Wings," *Journal of Aircraft,* Vol. 27, No. 5, 1990, pp. 473–475.

[29]Sychev, V. V., "Three Dimensional Hypersonic Gas Flow Past Slender Bodies at High Angles of Attack," *Journal of Applied Mathematics and Mechanics (USSR),* Vol. 24, Feb. 1960, pp. 296–306.

[30]Wentz, W. H., and MacMahon, M. C., "Further Experimental Investigations of Delta and Double Delta Flowfields at Low Speeds," NASA CR-714, Feb. 1967.

[31]Smith, J. H. B., "Calculations of the Flow over Thick, Conical, Slender Wings with Leading Edge Separation," Aeronautical Research Council R&M 3694, London, March 1971.